Pattern formation in large-aspect-ratio single-mode inhomogeneously broadened lasers

Eduardo Cabrera,* Oscar G. Calderón, and J. M. Guerra
Departamento de Optica, Universidad Complutense de Madrid, Ciudad Universitaria s/n, 28040 Madrid, Spain
(Received 26 April 2004; published 14 December 2004)

Pattern formation in large-aspect-ratio single-mode inhomogeneously broadened lasers is studied by means of the integro-differential Maxwell-Bloch equations. As the inhomogeneous linewidth increases, the neutral stability curve shows a relaxation in the traveling wave selection allowing structures with different sizes to grow. We have performed numerical simulations with a simplified model based on a few discrete groups of atoms at different resonant frequencies to observe transverse dynamics above threshold for good and bad cavity configurations. We obtain, in general, that close to threshold the inhomogeneous broadening leads to a more complex pattern in comparison to the homogeneous broadening case. At higher pumpings, a stabilization in the number of spatial frequencies taking part in the transverse pattern is found. The influence of the laser aperture on temporal dynamics is also studied. It is shown how the typical self-pulsing regime present in single-mode inhomogeneously broadened lasers is destroyed for a wide enough aperture.

DOI: 10.1103/PhysRevA.70.063808 PACS number(s): 42.65.Sf, 42.55.−f, 42.60.Jf, 42.60.Mi

I. INTRODUCTION

Instabilities in single-mode lasers have been a subject of intense research. The simplest laser system from both the experimental and theoretical point of view is the single-mode homogeneously broadened (SMHB) laser [1]. The first experiments showing instabilities in SMHB lasers were reported in 1985 by Klische and Weiss [2] in a far-infrared NH_3 laser. There are two conditions for observing instabilities (pulsing behavior or non-constant-intensity behavior) in these systems. First, the field decay rate κ must be larger than the sum of the polarization ($\gamma_\perp$) and population inversion ($\gamma_\parallel$) decay rates, i.e., $\kappa > \gamma_\perp + \gamma_\parallel$, which is usually called the bad cavity condition. Second, the pump value (the excitation level) must be larger than a certain threshold value. This is the well-known second laser threshold or instability threshold. Depending on the value of $\gamma \equiv \gamma_\parallel / \gamma_\perp$, the second threshold value is predicted to be between 9 and 20 times above the first laser threshold. So the instability threshold in SMHB lasers is very high, which makes the observation of these phenomena very difficult. In contrast, instabilities in single-mode inhomogeneously broadened (SMIB) lasers are experimentally more accessible since the second laser threshold is much lower in these lasers. In 1972, Casperson and Yariv observed undamped trains of pulses in a He-Xe laser [3]. In this work, this behavior was attributed to transient relaxation oscillations [4]. However, a few years later, Casperson derived an acceptable model to explain the self-pulsing behavior [5]. The physical origin of SMIB and SMHB laser instabilities is different [6]. In SMHB lasers, the nonlinear interaction of the field and polarization plays an important role in the onset of instabilities, whereas in SMIB lasers, the self-pulsing behavior is due to a self-organization process of the radiating dipoles in the laser medium [6]. More recent experiments in SMIB lasers were done by Abraham and co-workers [7–9]. They analyzed the instabilities in great detail using lasers similar to the ones used by Casperson, which are characterized by a small ratio of the population and polarization decay rates, i.e., $\gamma \ll 1$ ($\gamma = 0.05$ appropriate to the 3.51-μm He-Xe laser). As we mentioned above, these systems exhibit regular trains of pulses.

The first theoretical prediction of instabilities in SMIB lasers was given in 1973 by Idiatulin and Uspenskii [10]. By using a laser medium composed of two group of atoms with different resonant frequencies, they showed a change of the nature of the laser instability and a marked reduction of the threshold for the onset of pulsations. This type of model—based on a few discrete group of atoms—has been extensively used [11–14]. Following this approach, Meziane analyzed the effect of the strong velocity-changing collisions on the dynamics of a SMIB laser by including spectral cross-relaxation terms [15]. A reduction of both the first laser threshold and the second laser threshold was found. The theoretical study of instabilities in SMIB lasers is a difficult task in comparison to the case of SMHB lasers, since the inhomogeneous broadening leads to an infinite dimension system, the integro-differential Maxwell-Bloch equations. This system has been analytically and numerically analyzed [14,16–20]. In 1983, Graham and Cho constructed a simple (low-dimensional) model [21]. They reduced the integro-differential Maxwell-Bloch equations to a set of four differential equations by using macroscopic variables of the medium (total polarization and total population inversion). This simple model allows a straightforward analytical study of the instabilities in SMIB lasers [21]. Similar models based on this approach have been constructed by Meziane [6,22]. Bowden *et al.* studied the dynamics of a SMIB laser in a dense medium [23]. The local-field effects occurring in dense media reduce the range of continuous wave operation and lead to instabilities and chaos at much lower pumping levels. Other experimental single-mode inhomogeneously broadened systems that have showed instabilities are FIR lasers such as $C^{13}H^3F$ laser [12,24,25]. They are characterized by the radiative limit, i.e., $\gamma_\parallel \simeq \gamma_\perp$, so the bad cavity condition is more accessible in these lasers. For low excitation, they ex-

*Electronic address: ecabrera@fis.ucm.es; URL: http://www.ucm.es/info/laserlab

hibit periodic oscillations in their output intensity.

Most of the research in SMIB lasers has been based on the plane-wave approximation, that is, ignoring transverse effects in the medium or in the field. Furthermore, the few works concerning transverse effects have been devoted to the case of low Fresnel number (small-aspect-ratio) lasers, where the optical resonator imposes the geometry of the laser field, which can be expanded on a suitable basis of empty cavity modes. This Fresnel number is defined as $\mathcal{F}=\pi b^2/(\lambda L)$, where $2b$ is the laser aperture, λ the lasing wavelength, and L the resonator length. Based on the results of Lugiato and Milani [26], Abraham *et al.* found similar results in the steady-state behavior in the presence of a Gaussian transverse intensity profile in comparison to the plane-wave case [17]. Huyet *et al.* demonstrated that the breaking of the cylindrical symmetry of transverse patterns is relatively insensitive to whether the medium is homogeneously or inhomogeneously broadened [27]. Finally, Skryabin studied the dynamical transverse patterns in a laser operating in a pair of doughnut modes [28].

On the other hand, it is well-known that as the Fresnel number increases, the behavior of the system becomes more and more boundary-free, and the structure formation begins to be dominated by bulk parameters and nonlinearities of the active medium. Pattern formation and dynamics of transverse light patterns in large-aspect-ratio (high Fresnel number) lasers and other nonlinear resonators have been a field of intense research in recent years [29–40]. However, to our knowledge, the dynamics of transverse patterns in large-aspect-ratio SMIB lasers has not been studied. In this work we address this problem. The description is made by means of the semiclassical Maxwell-Bloch equations for a SMIB laser, assuming the rotating wave and the slowly varying amplitude approximations. In large-aspect-ratio SMHB lasers, it is well-known that the pattern selected just above threshold depends on the sign of the cavity detuning Δ [29,30,34]. For negative detuning (cavities tuned above resonance), the laser selects a transverse spatially homogeneous solution, whereas for positive detuning (cavities tuned below resonance), a traveling wave is selected. In this last case, the laser emission is off-axis which helps the laser to emit on resonance. This phenomenon has been experimentally observed [37,38].

Here, we analyze the influence of the inhomogeneous broadening on the laser transverse dynamics. The neutral stability curve obtained in the linear stability analysis of the nonlasing solution depends on the inhomogeneous linewidth. As this inhomogeneous linewidth increases the traveling wave selection is less relevant and a continuous laser field spectrum would be expected. We have performed numerical simulations to observe the pattern formation above threshold. Due to the complexity of the 3D integro-differential Maxwell-Bloch equations, the simulations have been developed by following the model of Idiatulin and Uspenskii [10], that is, based on a few discrete group of atoms at different resonant frequencies. We have analyzed both the good and the bad cavity configurations. In the good cavity limit, we find in general that the inhomogeneous broadening leads to a more complex pattern in comparison to the homogeneous broadening case. On the other hand, for the bad cavity limit, the simulations reveal that the pattern tends to be formed by several traveling waves for pumpings well above threshold. So, a roll intensity pattern is observed. Hence, in this case, we obtain that the SMIB laser, through the introduction of new atom packets under the gain profile, develops a more ordered pattern than the SMHB laser for the same parameters. We have also analyzed the effect of the transverse dynamics on the self-pulsing behavior typical of SMIB lasers and we have found that the spatial degrees of freedom destroy the self-pulsing regime.

The paper is organized as follows: In Sec. II we present the two-level Maxwell-Bloch equations for a single-mode inhomogeneously broadened laser. In Sec. III, we analyze how the inhomogeneous broadening affects the first laser threshold by doing a linear stability analysis of the nonlasing solution. The lasing solutions above threshold and their linear stability analysis are presented in Sec. IV. The numerical simulations are presented in Sec V. Finally, Sec. VI provides brief conclusions.

II. MODEL

The semiclassical two-level Maxwell-Bloch equations for a large-aspect-ratio inhomogeneously broadened laser, with plane and parallel mirrors in the rotating wave, slowly varying amplitude, and single longitudinal mode approximations are

$$\frac{\partial E}{\partial \tau} = ia\Delta_{\perp}E - \sigma E + \sigma \int d\Omega\, g(\Omega)P(\Omega), \tag{1}$$

$$\frac{\partial P(\Omega)}{\partial \tau} = -(1 + i\Delta + i\Omega)P(\Omega) + D(\Omega)E, \tag{2}$$

$$\frac{\partial D(\Omega)}{\partial \tau} = -\gamma\left[D(\Omega) - r + \frac{1}{2}[E^*P(\Omega) + EP(\Omega)^*]\right]. \tag{3}$$

E is the dimensionless envelope of the electric field. $P(\Omega)$ and $D(\Omega)$ are the dimensionless envelopes of the electric polarization, and the population inversion of each atom packet labeled by Ω. The frequency shift Ω from the center of the inhomogeneous line is scaled in units of the polarization decay rate $(\gamma_{\perp})$. $\gamma \equiv \gamma_{\parallel}/\gamma_{\perp}$ and $\sigma \equiv \kappa/\gamma_{\perp}$ are the population inversion decay rate and the cavity losses, respectively, also normalized with $\gamma_{\perp}$. $\Delta \equiv (\omega_{21}-\omega)/\gamma_{\perp}$ is the rescaled detuning between the atomic line center and frequency of the cavity mode. r represents the pumping parameter. Light diffraction is introduced by means of the transverse Laplacian term in the field equation, and is measured by the diffraction coefficient $a \equiv c^2/(2\omega\gamma_{\perp}b^2)$ where b is the spatial transverse size of the laser. $\Delta_{\perp} \equiv \partial_x^2 + \partial_y^2$ is the transverse Laplacian where x and y are normalized with the spatial scale b, i.e., the scaled (x,y) frame is the physical (x,y) window divided by the transverse aperture size b. The time τ is normalized versus the polarization decay rate $(\tau=\gamma_{\perp}t)$. $g(\Omega)$ is the normalized spectral distribution. The most common form is a Gaussian distribution which can be caused by thermal motion in a gaseous medium. Its expression, widely known, is

$$g(\Omega) = \frac{1}{(2\pi\sigma_D^2)^{1/2}} \exp(-\Omega^2/2\sigma_D^2), \tag{4}$$

where σ_D is in units of $\gamma_\perp$ and represents the width of the distribution. However, it is well-known that the spectral distribution can present deviations from that broadening, for instance, because of the presence of different isotopes, local variations of the crystal field, or impurities. But these deviations have little consequences, at least qualitatively [1]. It is for this reason, and because the Gaussian profile does not allow an analytical handling, why we have used a Lorentzian profile to reach the expressions we give in the next sections. In this case,

$$g(\Omega) = \frac{\sigma_D}{\pi} \frac{1}{\Omega^2 + \sigma_D^2}. \tag{5}$$

III. STABILITY OF THE NONLASING SOLUTION

We have studied the onset of the laser emission, that is, the first laser threshold. This can be done by the analysis of the stability of the nonlasing solution $E=0, P=0, D=r$ expanding the variables as Fourier series of transversal modes of wave vectors k. The following system of equations is obtained for each set of Fourier components $(\delta E_k, \delta P_k, \delta D_k)$:

$$\frac{\partial\, \delta E_k}{\partial\, \tau} = -\, iak^2 \delta E_k - \sigma \delta E_k + \sigma \int d\Omega\; g(\Omega)\, \delta P_k, \tag{6}$$

$$\frac{\partial\, \delta P_k}{\partial\, \tau} = -\,(1 + i\Delta + i\Omega)\, \delta P_k + r\, \delta E_k, \tag{7}$$

$$\frac{\partial\, \delta D_k}{\partial\, \tau} = -\,\gamma \delta D_k. \tag{8}$$

The last equation gives the trivial eigenvalue $\lambda = -\gamma$, which leads no instability. The other two yield the following equation for the eigenvalues:

$$\lambda + iak^2 + \sigma = \sigma r \int d\Omega \frac{g(\Omega)}{1 + \lambda + i(\Delta + \Omega)}. \tag{9}$$

At the first laser threshold $r_{\rm th}$, the real part of the eigenvalue λ changes from a negative value to a positive one (the instability condition), while the imaginary part gives the frequency of the temporal evolution of the growing instabilities $[\mathrm{Im}(\lambda) \equiv \lambda_I]$, i.e., a Hopf bifurcation takes place as in the homogeneous broadening case. Thus, the neutral stability curve will be obtained fixing $\mathrm{Re}(\lambda) = 0$. With this condition, and treating separately the real and imaginary parts of Eq. (9) we arrive to two equations which relate $r_{\rm th}, k$, and λ_I:

$$\lambda_I + ak^2 = -\,\sigma r_{\rm th} \int d\Omega \frac{g(\Omega)(\Delta + \Omega + \lambda_I)}{1 + (\Delta + \Omega\lambda_I)^2}, \tag{10}$$

$$1 = r_{\rm th} \int d\Omega \frac{g(\Omega)}{1 + (\Delta + \Omega\lambda_I)^2}. \tag{11}$$

For a Lorentzian distribution, these expressions can be solved analytically, giving

$$r_{\rm th} = (1 + \sigma_D)\left[1 + \left(\frac{\Delta - ak^2}{1 + \sigma + \sigma_D}\right)^2\right], \tag{12}$$

$$\lambda_I = -\left[\frac{(1 + \sigma_D)ak^2 + \sigma\Delta}{1 + \sigma + \sigma_D}\right]. \tag{13}$$

The previous expressions reveal the following main features.

(a) If the detuning Δ takes a negative value, the homogeneous transverse structure arises first, while a positive value of Δ causes the usual critical traveling wave with $k = \sqrt{\Delta/a}$ to appear. These are the same results of the homogeneous broadening case.

(b) The minimum value of the pump to obtain laser emission changes from 1 in the homogeneous broadening case to a greater value of $r_{\rm min} = (1 + \sigma_D)$.

(c) An increase of σ_D makes smaller the term that selects the transversal structure. If the inhomogeneous profile is wide enough the pump threshold can be almost independent of the wave vector k and of the detuning.

(d) The expression of λ_I gives the oscillation frequency of the first Fourier mode that appears on the onset of the laser emission. Note that the oscillation frequency depends on the inhomogeneous linewidth. As it happens in the homogeneous broadening case, the off-axis laser emission—with the critical traveling wave—helps the system to emit on resonance, i.e., the off-axis laser emission frequency is ω_{21}.

Figure 1 shows the behavior of the neutral stability curve for different widths of the spectral profile and both signs of the detuning. The figures are calculated with a Lorentzian profile but we have obtained the same behavior with a more realistic Gaussian distribution. It can be noted that a wider profile implies less restrictive selection for the wave vector k. For $\sigma_D = 10$ (see dotted line in Fig. 1) the neutral stability curve is almost plane which implies a broad spectrum in the transverse pattern. This result can be interpreted as a competition between different groups of frequencies under the inhomogeneous profile. Each of these groups has a different detuning $(\Delta + \Omega)$, and thus, we could associate to each packet the wave vector selected at threshold in the homogeneous broadening case for its detuning, i.e., $k = \sqrt{(\Delta + \Omega)/a}$. If the spectral profile $g(\Omega)$ is wide enough for allowing different groups of frequencies with similar strengths the resulting neutral stability curve will present a general smoothing. So then, the appearance of structures with different sizes and new complex patterns can be expected.

IV. SOLUTION ABOVE THRESHOLD

The system admits, above threshold, traveling waves solutions of the form

$$E = E_{\rm st} e^{i(\vec{k}\cdot\vec{x} + \omega_{\rm st}\tau)}, \quad P = P_{\rm st} e^{i(\vec{k}\cdot\vec{x} + \omega_{\rm st}\tau)}, \quad D = D_{\rm st}, \tag{14}$$

where $E_{\rm st}$ and $D_{\rm st}$ are real numbers whereas $P_{\rm st}$ is a complex quantity. Introducing the expressions (14) in Eqs. (1)–(3) and for a Lorentzian profile we can get the following expressions:

$$r = \xi(\sigma_D + \xi)\left[1 + \frac{(\Delta - ak^2)^2}{(1 + \sigma + \sigma_D)^2}\right], \tag{15}$$

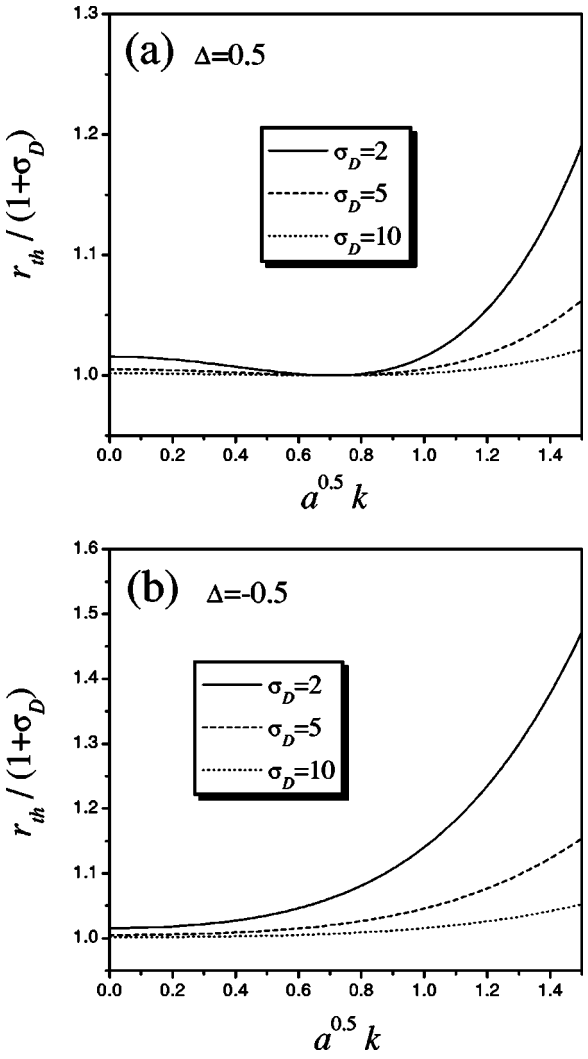

FIG. 1. General shape of the neutral stability curve, $r_{\mathrm{th}}(k)$, for an inhomogeneous linewidth $\sigma_D=2$ (solid line), $\sigma_D=5$ (dashed line), and $\sigma_D=10$ (dotted line), and for both signs of detuning (a) $\Delta=0.5$ and (b) $\Delta=-0.5$. The parameter $\sigma=1$. All these magnitudes are dimensionless.

$$\omega_{\mathrm{st}}=\frac{(\sigma_D+\xi)ak^2+\sigma\Delta\xi}{\sigma_D+\xi(1+\sigma)}, \tag{16}$$

$$P_{\mathrm{st}}=\frac{[1-i(\Delta+\Omega-\omega_{\mathrm{st}})]}{(\Delta+\Omega-\omega_{\mathrm{st}})^2+\xi^2}rE_{\mathrm{st}}, \tag{17}$$

$$D_{\mathrm{st}}=r\frac{1+(\Delta+\Omega-\omega_{\mathrm{st}})^2}{(\Delta+\Omega-\omega_{\mathrm{st}})^2+\xi^2}, \tag{18}$$

where $\xi=\sqrt{1+|E_{\mathrm{st}}|^2}$.

We analyze the stability of this steady state following the traditional lines of the linear stability analysis. We introduce in Eqs. (1)–(3) the solution

$$E=(E_{\mathrm{st}}+e_1e^{i\vec{q}\cdot\vec{x}}+e_2e^{-i\vec{q}\cdot\vec{x}})e^{i(\vec{k}\cdot\vec{x}+\omega_{\mathrm{st}}\tau)},$$

$$P=(P_{\mathrm{st}}+p_1e^{i\vec{q}\cdot\vec{x}}+p_2e^{-i\vec{q}\cdot\vec{x}})e^{i(\vec{k}\cdot\vec{x}+\omega_{\mathrm{st}}\tau)},$$

$$D=D_{\mathrm{st}}+de^{i\vec{q}\cdot\vec{x}}+d^*e^{-i\vec{q}\cdot\vec{x}}, \tag{19}$$

where e_1,e_2,p_1,p_2, and d are the perturbations, and $\vec{q}$ is the perturbation wave vector. Then we obtain $\partial_\tau\vec{v}=\mathcal{M}(\vec{k},\vec{q},r)\vec{v}$, where $\mathcal{M}$ is an infinite dimensional matrix and $\vec{v}$ denotes the column vector $(e_1,e_2^*,p_1,p_2^*,d)^T$. The time dependence of $\vec{v}$ is chosen as $e^{\lambda\tau}$, λ being the eigenvalues of $\mathcal{M}$. For a given $\vec{k}$ and r the traveling wave solution is stable if, for all values of $\vec{q}$, the matrix of the coefficients $\mathcal{M}$ has all its eigenvalues with negative real part. If any eigenvalue has positive real part, the solution represented by $(\vec{k},r)$ is unstable. Note that we have to assume a direction for the traveling wave $\vec{k}$ and consider perturbations at arbitrary directions relative to the fixed direction. Here, we will consider two cases: perturbations occurring along the direction of the traveling wave ($\vec{q}$ parallel to $\vec{k}$) which give 1D instabilities, and perturbations occurring at right angles of the traveling wave ($\vec{q}$ perpendicular to $\vec{k}$) which give 2D instabilities.

This stability analysis has been done numerically, showing no stable region in the plane (k,r), even for small values of σ_D such as less than unity. In other words, no stable transverse traveling wave solution is found for any pump value and any wave vector when we take into account an inhomogeneous broadening of the spectral profile. This result shows that more complex processes of competition between different growing waves must happen. But the pattern is not completely disordered just crossing the threshold, as it will be seen in the next section. This is because the new waves that grow faster have $\vec{q}\simeq 0$, not changing the original value of the wave vector present in the pattern.

V. NUMERICAL SIMULATIONS

The introduction of the integral on the medium's polarization makes the phase space infinitely dimensional. This is usually handled by fixing the number of frequency components under the gain profile, and increasing this number to obtain greater accuracy [14]. However, the presence of the transverse Laplacian introduces spatial degrees of freedom, which forces some approximations to be taken in order to make the problem numerically feasible. There have been two main strategies to do that, as it is discussed in the Introduction. One such strategy consists in limiting the discretization of the inhomogeneous profile into only a small number of groups of atoms at different resonant frequencies. Idiatulin and Uspenskii [10] showed that the consideration of two groups of atoms placed at symmetric positions under the spectral profile leads to a reduction of the second laser threshold with respect to the homogeneously broadened case. Of course, this model shows its inadequacy to describe the most part of the dynamical properties of the SMIB lasers. However, it has been demonstrated that the introduction of one or three more packets can make the model much more realistic [13]. Other strategy is the one proposed by Graham and Cho [21] in 1983. They generated macroscopic variables of the medium (total polarization and total population inversion). This change of variables solves the problem of the integral of the medium polarization in the equation of the

electric field, but leads to an infinite hierarchy of coupled equations that can be truncated by a judicious choice of some adjustable parameters. The approximation is introduced in this truncation, when we force to be zero one global variable, and approximate the value of one of these parameters using the stationary solution of the laser equations. But with the consideration of the spatial degrees of freedom, we have seen that the system admits solutions in the form given by Eq. (14), and the stationary state depends now on the wave vector $\vec{k}$, which is, in principle, unknown. Thus, to use the Graham and Cho approach, and fix the parameters, we must fix the value of $\vec{k}$ or leave the parameters as a function of k, which complicates the treatment. For this reason, we have found the first approximation more feasible to take into account the spatio-temporal dynamics of large-aspect-ratio lasers.

The most important question is which number of frequencies under the gain profile will be necessary to reach realistic results. We have found that an approximation of the system by 5 groups of atoms at different resonant frequencies can give, at least qualitatively, the behavior of the system. This election has been done taking the stability analysis of the steady state solution as a reference. In this analysis an eigenvalue problem is solved. This is an easier task than the integration of a system of partial differential equations so we can treat it with a high number of atomic frequencies in a normal computer. We have compared the behavior of the maximum eigenvalue versus the wave vector q of the perturbation added to the steady state solution, for different number of atomic frequencies n. No important qualitative changes appear for $n \geqslant 5$. Figure 2 shows some of these curves for different number of atomic frequencies. It must be noted that the analysis of the first laser threshold does not show great differences when changing the number of atomic frequencies, that is the reason why we have used the stability analysis of the steady state to choose the correct number of atomic packets. Thus, the minimum number of frequencies that can reproduce the main features of the spatio-temporal dynamics seems to be five, and this is the number of packets we have used.

In order to numerically solve the set of partial differential equations, we must remember that the transverse Laplacian variables have been scaled by the output aperture size b. The scaled window has been replaced by a 100×100 discrete numerical grid and applied a finite difference method. Periodic boundary conditions were programmed and a fourth order Runge-Kutta algorithm was used in the temporal variable. The system starts with small-amplitude random initial conditions and runs for times much larger than the characteristic relaxation times.

Two regimes have been explored: the good cavity configuration ($\sigma < 1$) and the bad cavity limit where the photon losses dominate the evolution of the magnitudes ($\sigma > 1$). It is in this last limit where a more rich behavior has been found in previous works from the point of view of the temporal dynamics. The detuning value has been fixed to $\Delta = 1.0$ and a diffraction coefficient equal to $a = 5 \times 10^{-4}$ has been used.

A. Good cavity limit, $\sigma = 0.5, \gamma = 0.2$

The inhomogeneous linewidth σ_D has been varied until a value of 5.0. For all of these cases and for values of the pump parameter r slightly greater than the threshold r_{th} a traveling wave appears, being its wave vector close to $\sqrt{\Delta/a}$. When r is increased new structures appear and the intensity pattern shows a more complicated shape, although the critical traveling wave is still present. Some examples are shown in Fig. 3 where the intensity field (first column), the phase field (second column), and the power spectrum (third column) are plotted for different values of the inhomogeneous linewidth (σ_D). All these figures correspond to the same pump value above threshold, i.e., the same ratio r/r_{th}, close to 1.7. For this pump value the laser pattern at $\sigma_D = 0$ (homogeneous broadening) is the critical traveling wave. For $\sigma_D = 1$ (first row in Fig. 3) we obtain the same pattern as that corresponding to the homogeneous broadening case, i.e., the critical traveling wave ($k = \sqrt{\Delta/a}$). The sequence of patterns for increasing σ_D shows how a wider profile favors the growing of new waves. In principle, these new contributions have wave vectors close to the critical one, and they simply modulate the intensity and the phase field patterns (see second row in Fig. 3 with $\sigma_D = 2.0$). Increasing a little bit the width of the inhomogeneous distribution, this modulation becomes deeper, and the system tends to form a roll pattern as can be seen for $\sigma_D = 3.0$ (see third row in Fig. 3). The new wave vectors are still close to the critical wave, and this is still present. But just for $\sigma_D = 3.5$ (see fourth row in Fig. 3), a

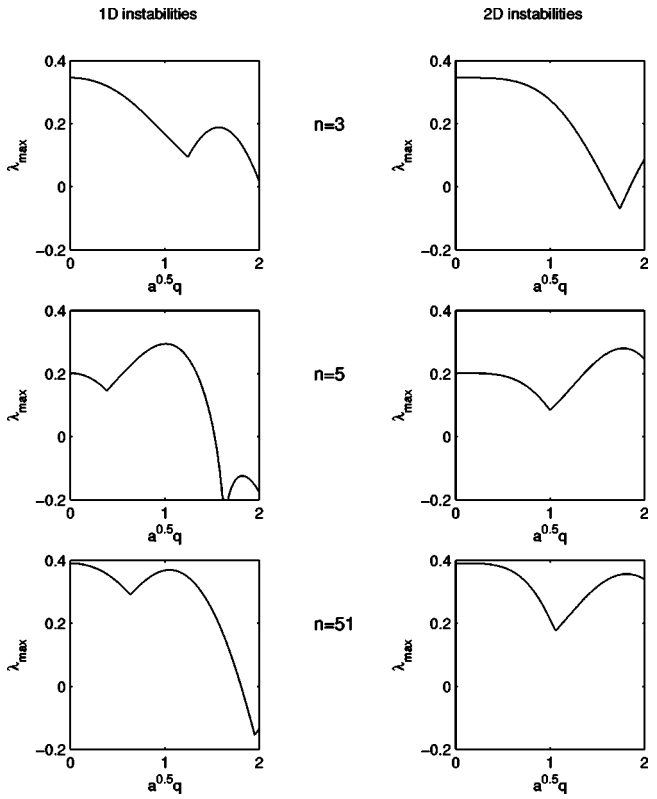

FIG. 2. Maximum eigenvalue $\lambda_{\max}$ vs the wave vector q of the perturbation in the stability analysis of the stationary solution, for different number n of atom packets: $n=3$ (first row), $n=5$ (second row), and $n=51$ (third row). The last case is equivalent to the continuous model of Eqs. (1)–(3). Left column shows $\lambda_{\max}$ when $\vec{q}$ is parallel to $\vec{k}$ (1D instabilities) and right column when $\vec{q}$ is perpendicular to $\vec{k}$ (2D instabilities). All the magnitudes are dimensionless.

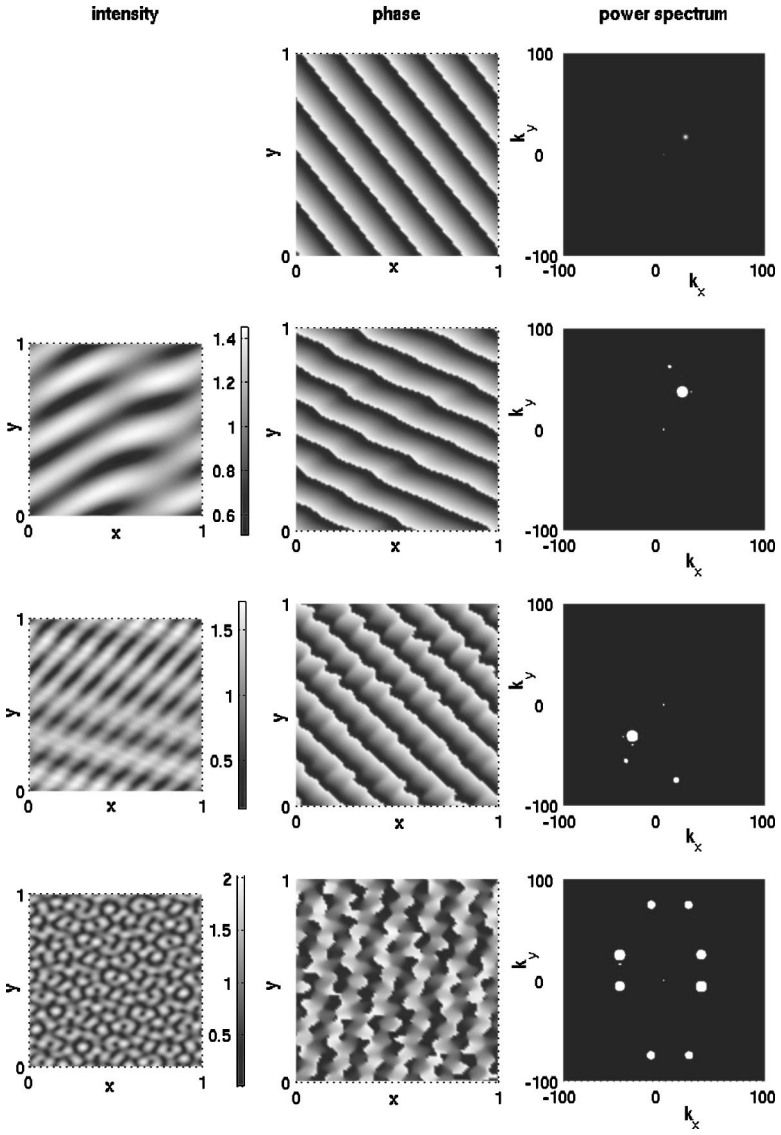

FIG. 3. Instantaneous intensity field (first column), phase field (second column), and power spectrum (third column) for different values of the inhomogeneous linewidth σ_D: $\sigma_D=1$ (first row), $\sigma_D=2.0$ (second row), $\sigma_D=3$ (third row), and $\sigma_D=3.5$ (fourth row). The rest of parameters are $\sigma=0.5$, $\gamma=0.2$, $\Delta=1.0$, $a=5\times10^{-4}$, and $r/r_{\mathrm{th}}=1.7$. The phase takes values from $-\pi$ to π in all the figures. All the magnitudes are dimensionless.

puzzle pattern can be seen, due to the presence of eight single waves. Thus, even a small inhomogeneous broadening of the spectral profile can give a very different spatial distribution of the intensity in comparison to the homogeneous broadening case.

Although we have obtained a more complex spatial profile due to the presence of the inhomogeneous broadening, the critical traveling wave persists in the spatio-temporal dynamics. This can be explained by means of the stability analysis of the traveling waves which indicates that the new waves that grow faster have $q\simeq0$, as it is mentioned in the previous section.

B. Bad cavity limit, $\sigma=5$

For this configuration, where field losses are greater than polarization decay, we have focused the study of two systems previously analyzed in the temporal case: the He-Xe laser [3] and the FIR laser [12,24,25]. In both $\sigma=5.0, \sigma_D=5.0$, while $\gamma=0.05$, for the forward system, and $\gamma=1.0$ for the latter. A very detailed study of the temporal evolution of these type of lasers can be found in Ref. [13]. In particular, two main regimes can be seen depending on the value of $\gamma=\gamma_{\parallel}/\gamma_{\perp}$. If this ratio is close to zero, the intensity can display a self-pulsing regime for high enough values of pumping, whereas for values of γ close to unity, no train of pulses appear and the dynamics consists of regular oscillations for not very high pump values.

We have seen also some differences in the evolution of the pattern for these two systems. Let us start analyzing the case with $\gamma=1$ for pump values close to the first threshold where the critical traveling wave is the only solution appearing in the homogeneous broadening case ($\sigma_D=0$). For an inhomogeneous spectral profile with $\sigma_D=5.0$, the critical traveling wave ($k=\sqrt{\Delta/a}$) appears when $r/r_{\mathrm{th}}\simeq1.0$ (see first row in Fig. 4). But for pumpings a little bit higher (even just 1.1 times the pump threshold), the system develops different domains of traveling waves separated by defects, which causes the appearance of two rows of zeros in the intensity pattern (see second row in Fig. 4). So, we have found again that the inhomogeneous broadening leads to a more complex

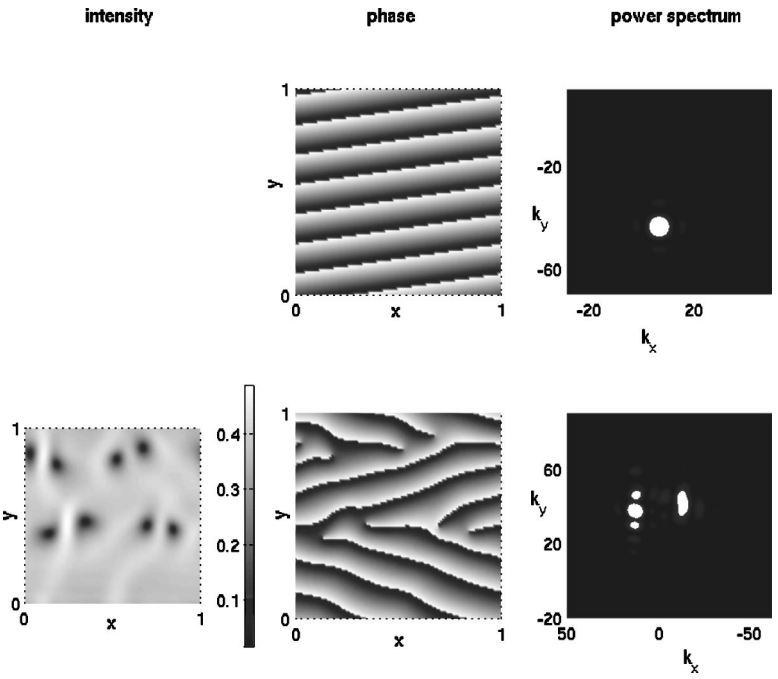

FIG. 4. Instantaneous intensity field (first column), phase field (second column), and power spectrum (third column) for different values of pumping: $r/r_{\mathrm{th}}=1.0$ (first row), and $r/r_{\mathrm{th}}=1.1$ (last row). The rest of parameters are $\sigma=5$, $\gamma=1$, $\Delta=1.0$, $a=5\times10^{-4}$, and $\sigma_D=5$. The parameters correspond to the FIR laser. All the magnitudes are dimensionless.

behavior in comparison to the homogeneous broadening case.

We are also interested in the spatio-temporal behavior of the SMIB laser for further pump values. An increase in the pumping to $r\simeq 2r_{\mathrm{th}}$ reveals the presence of rolls in the intensity pattern, due to the contribution of more waves. This is shown in the first row of Fig. 5. This result agrees with the stability analysis which shows a faster growing for new traveling waves with wave vectors close to the double of the critical one. For comparison purpose, we also present in this figure (second row) the result with the homogeneous broadening which shows a very complex pattern forming by several defects. Then, at higher pump values we have found how the SMIB laser, through the introduction of new atom packets under the gain profile, develops a more ordered pattern than the SMHB laser.

Let us study the case with $\gamma=0.05$. In this case, the pattern follows a different evolution than the previous one. For pumpings very close to the threshold value the system maintains the transversal critical wave. This simple spatial configuration disappears for a pump value close to 1.3 times the threshold, as it can be seen in the first row in Fig. 6. For this pumping the spatial intensity profile presents rolls due to the contribution of two waves, with wave vectors close to the critical one and to the double of its value. In the homogeneous broadening case, the critical traveling wave also disappears for the same pumping ($r\simeq 1.3r_{\mathrm{th}}$). The corresponding pattern is shown in the second row in Fig. 6. So, for the SMIB He-Xe laser ($\gamma=0.05$), the bifurcation to more complex patterns takes place for the same pump value above threshold as in the SMHB laser with the same parameters. Note that the inhomogeneous broadening leads to a more

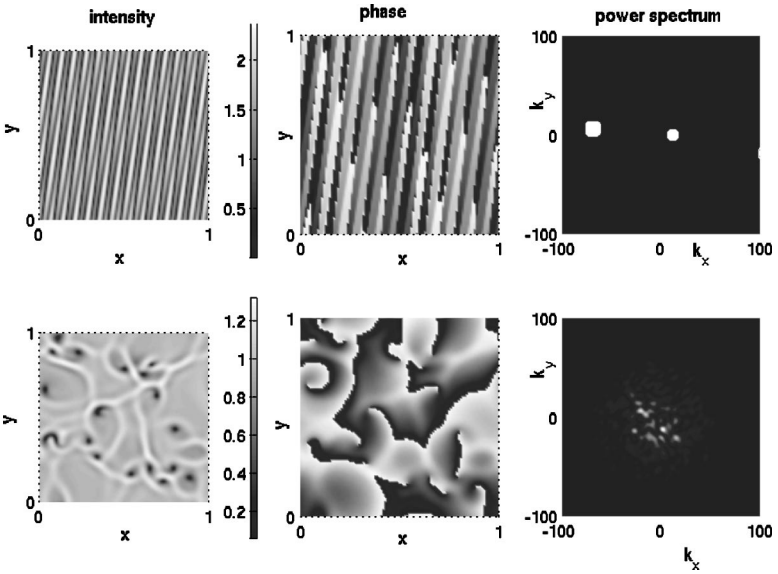

FIG. 5. Instantaneous intensity field (first column), phase field (second column), and power spectrum (third column) for $r/r_{\mathrm{th}}=2$. The first row corresponds to the FIR laser (see parameters in Fig. 4). The second row is the homogeneous broadening case ($\sigma_D=0$) for the same parameters. All the magnitudes are dimensionless.

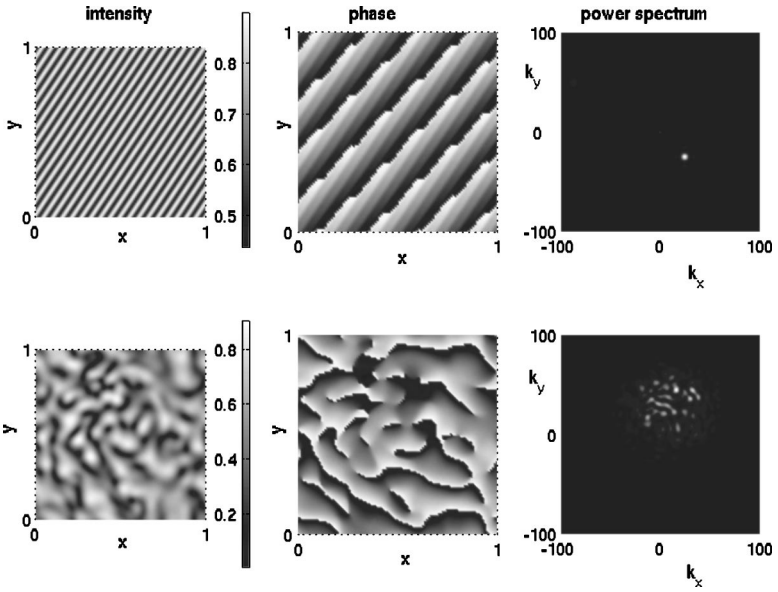

FIG. 6. Instantaneous intensity field (first column), phase field (second column), and power spectrum (third column) for $r/r_{\mathrm{th}}=1.3$. The rest of parameters are $\sigma=5$, $\gamma=0.05$, $\Delta=1.0$, $a=5\times10^{-4}$, and $\sigma_D=5$. The parameters correspond to the He-Xe laser (first row). The second row is the homogeneous broadening case ($\sigma_D=0$) for the same parameters. All the magnitudes are dimensionless.

regular spatial structure—forming by two waves—than the homogenous broadening. This trend also occurs for higher pump values as is shown in Fig. 7.

These results may suggest a stabilization in the number of the traveling waves taking part in the pattern for the inhomogeneous broadening case, even though it seems that would be easier for the system to generate new structures with different sizes, due to the lesser difference in the threshold to grow for the new waves with different wave vectors than the critical one.

C. Effect of the laser aperture on the dynamics

The dynamics of large-aspect-ratio lasers are influenced by bulk parameters and non-linearities of the medium, as it is mentioned in the Introduction. This influence changes not only the spatial profile of the output intensity but also the temporal behavior of both global and local intensity in comparison to the spatio-temporal behavior in small-aspect-ratio lasers. We have studied how this transition takes place for a case where it was experimentally found, for small-aspect-ratio systems, a self-pulsing regime [9]. Then, we used the parameters of the He-Xe laser of Ref. [9]. In this case, the inhomogeneous linewidth equals $\sigma_D=3.72$, $\sigma=4.67$, and $\gamma=0.183$. The comparison of our numerical simulations with these experimental results can also be used to test the model based on 5 atom packets with different resonant frequencies. The diffraction parameter a has been changed from the value used in previous sections ($a=5\times10^{-4}$) to a value of 0.4. This last value of a corresponds with an estimate made for the small-aspect-ratio laser used in the mentioned reference (Ref. [9]). Figure 8 shows the temporal behavior of global intensity (left column), local intensity (central column), and also the pattern intensity (right column) for different laser apertures, i.e., different values of a. In this figure, in order to compare in the same scale the numerical patterns obtained

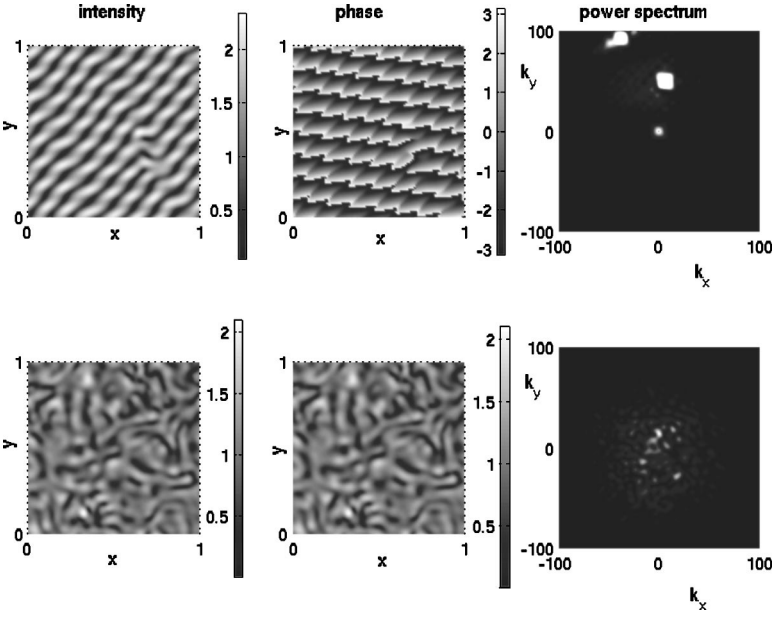

FIG. 7. Instantaneous intensity field (first column), phase field (second column), and power spectrum (third column) for $r/r_{\mathrm{th}}=2$. The first row corresponds to the He-Xe laser (see parameters in Fig. 6). The second row is the homogeneous broadening case ($\sigma_D=0$) for the same parameters. All the magnitudes are dimensionless.

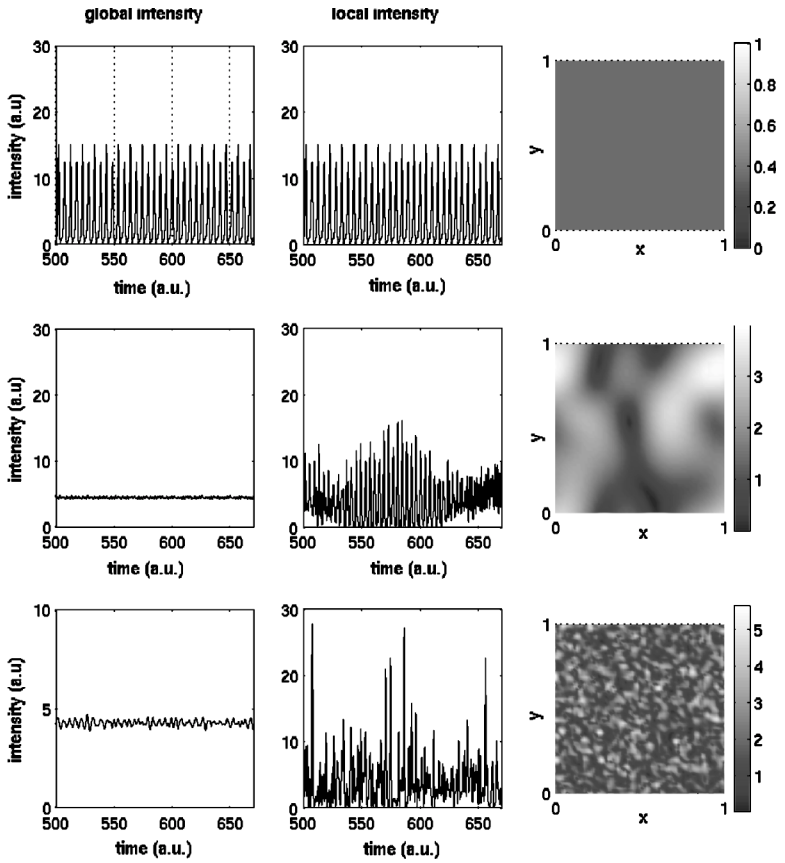

FIG. 8. Temporal evolution of global intensity (left column), local intensity (central column) and transverse pattern intensity (right column) for different values of diffraction parameter a. First row correspond to $a=0.4$, second row to $a=0.04$, and last row to $a=5\times10^{-4}$. The parameters correspond to the He-Xe laser used in Ref. [9]. All the magnitudes are dimensionless.

for the different sizes b, we must multiply the size shown in the figure by the scale factor b corresponding to each one. For $a=0.4$, that is, the experimental situation of Ref. [9], the results of our simulations are shown in the first row in Fig. 8. In agreement with the experiments, a self-pulsing regime is obtained and the global and local intensity follow the same behavior. We have compared the power spectrum obtained with those experimentally observed in Ref. [9]. For a similar position above threshold $(r/r_{\mathrm{th}}\sim3)$, both spectra show the same frequency for the main peak (20 MHz approx.). Thus, the model based on 5 different resonant frequencies can lead to results not only qualitatively but quantitatively accurate. In this situation, the intensity pattern consists of a true homogenous profile which corresponds to the homogeneous solution. The system chose this solution because any transverse wave is inhibited by the smallness of the physical transverse window. So this limit matches with the plane-wave approximation. If we reduce the diffraction parameter a, or in other words, if we increase the laser aperture b, the self-pulsing regime disappears. The second row shows the case where $a=0.04$. Now, the global intensity shows a very different behavior from the local intensity: the global intensity shows a constant contribution with a small irregular oscillation, whereas the local intensity displays a very much more complex behavior. However, the power spectrum of the local intensity still shows a peak placed close to 20 MHz which can be seen as a remnant of the self-pulsing behavior. The pattern presents some structures which become smaller as the diffraction parameter reduces its value. Finally, in the third row, $a=5\times10^{-4}$ is used. The local intensity is much more disordered, and the orderly self-pulsing contribution present in the previous cases is now buried under the wide global power spectrum. We must point out that this result indicates that the self-pulsing regime is not present in the local intensity which means that the disappearance of the self-pulsing is not caused by an unlocked dephasing between the different contributions of the pixels in which the transversal plane is divided. There is still the possibility that the increase of the laser aperture changed the region of pumping where the self-pulsing regime is found. But the different tests we have made to localize this region have failed, which makes this possibility improbable. The temporal features found at larger laser apertures indicate that the transverse effects are playing an important role on the dynamics. In fact, a very complex intensity pattern can be seen as the laser aperture increases.

VI. CONCLUSIONS

The transverse pattern of a SMIB laser with large-aspect-ratio has been analyzed in the first laser threshold. Analytical expressions for this threshold and for the stationary solutions are given using a Lorentzian spectral distribution. These expressions show how the presence of an inhomogeneous broadening in the gain profile not only increases the value of

the pump necessary for the beginning of the laser emission, but also relaxes the selection of a wave vector. It also changes the stability of the stationary solutions, making them unstable for the whole plane (k,r). But in spite of this, it does not mean that the transverse critical wave does not appear as it is shown in the simulations.

The SMIB laser is usually studied by the integro-differential Maxwell-Bloch equations, which makes the system infinite dimensional. Adding the spatial degrees of freedom to an accurate discretization of the gain distribution would make the system untreatable. For that reason, a model with only five atom packets with different resonant frequencies has been tested analyzing the stability of the stationary solution of the system. This type of approximation—based on a few discrete groups of atoms—has been already used in the study of the temporal dynamics of SMIB lasers in the plane-wave approximation, reproducing the behavior of the system even quantitatively in some cases. In our case (large-aspect-ratio lasers, and for the inhomogeneous linewidths studied), it can be seen that this simple model reproduces qualitatively the behavior of the maximum eigenvalue with the wave vector of the perturbation added to the stationary solution. Thus, we have developed simulations using this simple model which is expected to reproduce the spatio-temporal dynamics in the large-aspect-ratio SMIB lasers.

The transverse pattern of the system has been studied with this model for both good and bad cavity configurations. The good cavity configuration shows the presence of the critical transverse wave for small values of pumping independently of the value of the inhomogeneous width (up to a value of five times the homogeneous linewidth). But for a greater value of the pump, increasing this width leads to the appearance of new contributions in the power spectrum of the transversal field distribution. For instance, puzzles patterns appear for a width just 3.5 times the width of an homogeneous atom packet. For this pump value and in the absence of the inhomogeneous broadening the pattern shows the critical traveling wave. Thus, even a small inhomogeneous broadening of the spectral profile can give a very different spatial distribution of the intensity in comparison to the homogeneous broadening case.

For a bad cavity configuration the study has been focused on two systems widely analyzed in the plane-wave approximation, FIR lasers and He-Xe lasers. The simulations done for the parameters corresponding to these two systems show some differences in the laser pattern, mainly close to threshold. For the FIR laser, the transition from the pattern selected just at the first laser threshold (the critical traveling wave) to a more complex pattern occurs for a pump value very close to the threshold one. So, the inhomogeneous broadening leads to a more complex behavior close to threshold in comparison to the homogeneous broadening case. This phenomenon does not appear in the He-Xe laser, where the bifurcation to a more complex pattern takes place for a higher pump value, being the same as happens in the SMHB laser with the same parameters. At higher pumpings (well above threshold), a similar pattern is obtained at both types of SMIB laser analyzed. This laser pattern is formed by some traveling waves. As a consequence of this, the intensity develops a roll pattern. This trend has been compared with the behavior of the SMHB laser for the same set of parameters, showing a much more complicated pattern for this last case in the same range of pumping. Thus, it seems that even the presence of an inhomogeneous broadening relaxes the difference between the threshold of different waves, the system stabilizes the number of components that participate in the transverse profile for pumpings not very far from the threshold. Only a small number of different sizes is present in the pattern.

Finally, we have predicted the influence of the transverse effects in a He-Xe laser, on the self-pulsing behavior. We found that a wider aperture destroys the self-pulsing regime and tends to favor smaller structures and a much more complex spatiotemporal dynamics. The transition to this complex behavior occurs smoothly, and despite the irregular shape of the temporal evolution of the local intensity, for intermediate values of the diffraction coefficient a, the spectra of local irregular evolution still shows the characteristic frequency of self-pulsing dynamics. It is worth mentioning that the frequency of the self-pulsing regime obtained through the simplified model used in this work agrees with the experimentally observed frequency.

ACKNOWLEDGMENT

This work was supported by Project No. BFM2003-06292 (Spain).

[1] N. B. Abraham, L. A. Lugiato, and L. M. Narducci, J. Opt. Soc. Am. B **2**, 7 (1985).
[2] W. Klische and C. O. Weiss, Phys. Rev. A **31**, 4049 (1985).
[3] L. W. Casperson and A. Yariv, IEEE J. Quantum Electron. **QE-8**, 69 (1972).
[4] A. Yariv, *Quantum Electronics*, 2nd ed. (Wiley, New York, 1975), p. 277.
[5] L. W. Casperson, IEEE J. Quantum Electron. **QE-14**, 756 (1978); Phys. Rev. A **21**, 911 (1980).
[6] B. Meziane, Opt. Commun. **75**, 287 (1990).
[7] M. Maeda and N. B. Abraham, Phys. Rev. A **26**, 3395 (1982).
[8] R. S. Gioggia and N. B. Abraham, Phys. Rev. Lett. **51**, 650 (1983); Opt. Commun. **47**, 278 (1983); Phys. Rev. A **29**, 1304 (1984).
[9] M. F. H. Tarroja, N. B. Abraham, D. K. Bandy, and L. M. Narducci, Phys. Rev. A **34**, 3148 (1986).
[10] V. S. Idiatulin and A. V. Uspenskii, Radio Eng. Electron. Phys. **18**, 422 (1973).
[11] N. I. Polushkin, P. A. Khandokhin, and Ya. I. Khanin, Kvantovaya Elektron. (Moscow) **10**, 1461 (1983) [Sov. J. Quantum Electron. **13**, 950 (1983)].
[12] N. B. Abraham, D. Dangoisse, P. Glorieux, and P. Mandel, J. Opt. Soc. Am. B **2**, 23 (1985).
[13] B. Meziane and H. Ladjouze, Phys. Rev. A **45**, 3150 (1992).

[14] B. Meziane, Phys. Rev. A **48**, 2346 (1993).
[15] B. Meziane, Phys. Rev. A **47**, 4430 (1993).
[16] L. A. Lugiato, L. M. Narducci, D. K. Bandy, and N. B. Abraham, Opt. Commun. **46**, 115 (1983).
[17] N. B. Abraham, L. A. Lugiato, P. Mandel, L. M. Narducci, and D. K. Bandy, J. Opt. Soc. Am. B **2**, 35 (1985).
[18] L. W. Casperson, J. Opt. Soc. Am. B **2**, 62 (1985).
[19] Ji-yue Zhang, H. Haken, and H. Ohno, J. Opt. Soc. Am. B **2**, 141 (1985).
[20] S. Hendow and M. Sargent, J. Opt. Soc. Am. B **2**, 84 (1985).
[21] R. Graham and Y. Cho, Opt. Commun. **47**, 52 (1983).
[22] B. Meziane, *OSA Proceedings on Nonlinear Dynamics in Optical Systems*, edited by N. B. Abraham, E. Garmire, and P. Mandel (Optical Society of America, Washington, DC, 1991), Vol. 7, p. 519.
[23] C. M. Bowden, S. Singh, and G. P. Agrawal, J. Mod. Opt. **42**, 101 (1995).
[24] N. M. Lawandy and G. A. Knoepf, IEEE J. Quantum Electron. **QE-16**, 701 (1980); N. M. Lawandy, *ibid.* **QE-18**, 1992 (1982).
[25] C. O. Weiss, J. Opt. Soc. Am. B **2**, 137 (1985); C. O. Weiss and W. Klische, Opt. Commun. **51**, 47 (1984).
[26] L. A. Lugiato and M. Milani, Z. Phys. B: Condens. Matter **50**, 171 (1983).
[27] G. Huyet, C. Mathis, H. Grassi, J. R. Tredicce, and N. B. Abraham, Opt. Commun. **111**, 488 (1994).
[28] D. V. Skryabin, Quantum Semiclassic. Opt. **8**, 485 (1996).
[29] P. Coullet, L. Gil, and F. Rocca, Opt. Commun. **73**, 403 (1989).
[30] P. K. Jakobsen, J. V. Moloney, A. C. Newell, and R. Indik, Phys. Rev. A **45**, 8129 (1992).
[31] D. Dangoisse, D. Hennequin, C. Lepers, E. Louvergneaux, and P. Glorieux, Phys. Rev. A **46**, 5955 (1992).
[32] F. T. Arecchi, S. Boccaletti, P. L. Ramazza, and S. Residori, Phys. Rev. Lett. **70**, 2277 (1993).
[33] Q. Feng, J. V. Moloney, and A. C. Newell, Phys. Rev. A **50**, R3601 (1994).
[34] P. K. Jakobsen, J. Lega, Q. Feng, M. Staley, J. V. Moloney, and A. C. Newell, Phys. Rev. A **49**, 4189 (1994).
[35] G. Huyet, MC. Martinoni, J. R. Tredicce, and S. Rica, Phys. Rev. Lett. **75**, 4027 (1995).
[36] I. Fischer, O. Hess, W. Elsäßer, and E. Göbel, Europhys. Lett. **35**, 579 (1996).
[37] K. Staliunas, G. Slekys, and C. O. Weiss, Phys. Rev. Lett. **79**, 2658 (1997).
[38] S. P. Hegarty, G. Huyet, J. G. McInerney, and K. D. Choquette, Phys. Rev. Lett. **82**, 1434 (1999).
[39] F. Encinas-Sanz, I. Leyva, and J. M. Guerra, Phys. Rev. Lett. **84**, 883 (2000).
[40] Y. F. Chen and Y. P. Lan, Phys. Rev. A **64**, 063807 (2001); **65**, 013802 (2002).